ARCHIVES OF ELECTRICAL ENGINEERING VOL. 69(1), pp. 215–231 (2020)

DOI 10.24425/aee.2020.131769

Novel soft-start method for three-phase voltage source rectifier based on virtual resistor control

KAIZHONG HE, HONGSHENG SU

School of Automation and Electrical Engineering, Lanzhou Jiaotong University
Anning West Road 88, Anning District, Lanzhou, 730070, China
e-mail: 1050325747@qq.com

(Received: 08.04.2019, revised: 18.10.2019)

Abstract: The existence of inrush current poses a significant problem during the start-up process within three-phase voltage-source rectifiers. To address this problem, this study proposes a strategy to suppress the inrush current effectively based on the virtual-resistor-control method, while preventing the increase in cost of the system and complexity of the algorithm. First, a mathematical model is established based on the dq coordinate frame, and the primary cause of the inrush current is analyzed. Then, the design process of the virtual-resistor-control method is detailed. Finally, the accuracy and effectiveness of the proposed method are verified by simulations and experiments. The results show that the inrush current can be more than two times the rated current before the addition of the virtual resistor. The start-up process can be realized without the inrush current after the addition of the virtual resistor, it does not need to increase hardware costs, there is no secondary inrush current, and the sensitivity of the parameters and the complexity of control are low.

Key words: equipment safety, inrush current, rectifier, stable operation, virtual resistor

1. Introduction

With the development of green energy technology, power electronic converters have received much attention [1–4]. Three-phase voltage-source rectifiers (VSRs) have many advantages, such as low harmonic content, unity-power factor, and controllable DC voltage. VSRs have been widely used in middle- and high-power applications.

Usually, the control method with voltage and current proportional-integral (PI) regulators in a synchronous rotating frame is applied to VSRs. However, when the VSR is started, an inrush current is easily caused. Usually, the inrush current value far exceeds the rated current, which increases the current stress of power devices, and it threatens the safe, reliable operation of power electronic devices and the stability of the power grid.

To solve this problem, some scholars have put forward the corresponding control strategies [5–14]. At present, starting resistor methods are commonly used to achieve soft starting [12].

In a previous study [5], the current reference value was assigned according to the slow ramp, so that the DC voltage rose slowly. When it increased to 90% of the expected value, the external voltage loop was added to control the VSR. In another study [6], the method of setting the slow ramp reference value with a fixed slope was replaced by a continuous three-part curve to suppress the inrush current. In a third study [7], the inrush current was eliminated by setting parameters before adding the driving signal to the power transistor and setting the current reference according to a slow ramp. The slow ramp reference value was adopted in studies [5–7]. Although this method can restrain the inrush current to some extent, it reduces the dynamic response speed, and the actual value cannot track the given reference value completely. Therefore, the effect is greatly influenced by the control parameters.

In study [8], at the beginning of the grid connection, the lower arm is controlled to turn on; the duty cycle increases gradually and reaches normal value according to the fixed slope, and then the upper arm is controlled to turn on after the DC side voltage rises to the rated value. In previous study [9], an interval-dividing control method was proposed to reduce the impulse current by detecting the region where the impulse current is located and controlling the switching device switching on and off accordingly. The two methods mentioned above forcibly control the turn-on and turn-off processes of the switching device, but this can lead to an increase in switching device loss and a decrease in service life.

In other research [10], the opposite direct current component attenuated exponentially with a fixed time constant was injected into the modulation wave to reduce the inrush current in the start-up process. However, the detection algorithm is complex and involves time delay, so the effect is not ideal. In reference [11], an initial feedforward slow-start method with negative feedback from a high-pass filter was proposed, but, in fact, the starting impulse current was a low-frequency response, so the control effect was not ideal. In reference [12], a method of increasing the starting resistor performance was used to suppress the inrush current, but it increased the cost of the system. In other work [13], a method to improve the start-up performance under amplitude and phase control was proposed. Voltage predictive control was added to reduce the impulse current, but the algorithm for voltage predictive control is cumbersome and easily affected by parameters. An additional pre-synchronization method based on a phase-locked loop was proposed in [14] to realize the synchronization of voltage amplitude and phase to reduce the inrush current, but the control algorithm is complex.

The aforementioned studies have managed to reduce the inrush current to some extent, but all the methods employed to date possess shortcomings. In this study, the causes of the starting inrush current are theoretically analyzed in detail, and a new strategy is proposed to suppress the generation of inrush current at a fundamental level.

2. Analysis of the generation mechanism of inrush current

Fig. 1 shows the main circuit diagram of a three-phase VSR. Here, e_a, e_b, and e_c are three-phase AC voltages; i_a, i_b, and i_c are three-phase AC currents; u_a, u_b, and u_c are the input voltages of the three-phase VSR bridge arm; R and L are the AC side resistors and inductors, respectively;

C_{dc} and R_L are DC side capacitors and load resistors, respectively; U_{dc} is the DC side capacitive voltage; and rm i_{dc} and i_L are the DC side current and load current, respectively. The main circuit reference direction is shown in Fig. 1.

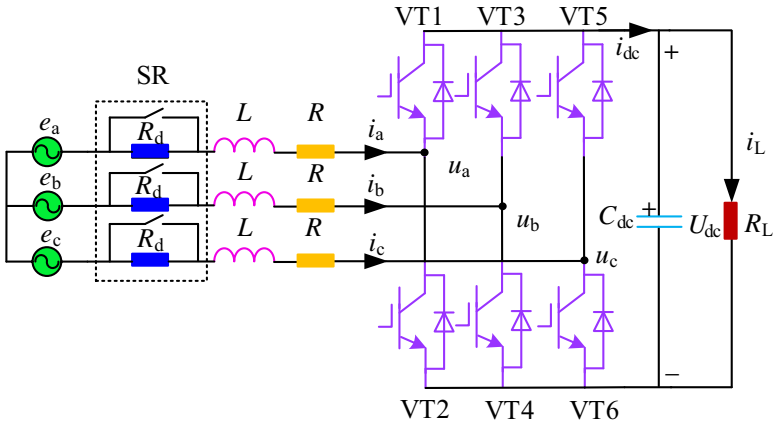

Fig. 1. Main circuit diagram of the three-phase VSR

According to Kirchhoff's voltage law, the dynamic equation of a three-phase VSR can be obtained as:

$$L\frac{\mathrm{d}\boldsymbol{I}}{\mathrm{d}t} + R\boldsymbol{I} = \boldsymbol{E}_g - \boldsymbol{U}_s, \tag{1}$$

where $\boldsymbol{I}$ is the current vector, $\boldsymbol{I} = [i_a\ i_b\ i_c]^T$, $\boldsymbol{U}_s$ is the input voltage vector of the VSR bridge arm, $\boldsymbol{U}_s = [u_a\ u_b\ u_c]^T$, and $\boldsymbol{E}_g$ is the voltage vector of the power grid, $\boldsymbol{E}_g = [e_a\ e_b\ e_c]^T$.

The transformation matrix of synchronous rotating coordinates is:

$$\boldsymbol{T}_{abc/dq} = \frac{2}{3}\begin{bmatrix} \cos\theta & \cos(\theta - 220°) & \cos(\theta + 220°) \\ \sin\theta & \sin(\theta - 220°) & \sin(\theta + 220°) \end{bmatrix}, \tag{2}$$

where θ is the phase of the grid voltage.

Eq. (1) in a synchronous rotating coordinate system is:

$$\begin{cases} i_d R + L\dfrac{\mathrm{d}i_d}{\mathrm{d}t} = e_d - u_d + \omega L i_q \\ i_q R + L\dfrac{\mathrm{d}i_q}{\mathrm{d}t} = e_q - u_q + \omega L i_d \end{cases}. \tag{3}$$

Here, e_d and e_q are the d-axis and q-axis components of three-phase AC voltage, respectively, i_d and i_q are the d-axis and q-axis components of three-phase AC current, respectively, u_d and u_q are the d-axis and q-axis components of the bridge arm input voltage, respectively, and ω is the angular frequency of the fundamental voltage wave in a power grid.

Eq. (3) shows that the d-axis and the q-axis are coupled and need to be decoupled, if:

$$\begin{cases} u'_{\mathrm{d}} = e_{\mathrm{d}} - u_{\mathrm{d}} + \omega L i_{\mathrm{q}} \\ u'_{\mathrm{q}} = e_{\mathrm{q}} - u_{\mathrm{q}} + \omega L i_{\mathrm{d}} \end{cases}. \tag{4}$$

Bringing Eq. (4) into Eq. (3), one can obtain that:

$$\begin{cases} i_{\mathrm{d}} R + L \dfrac{\mathrm{d}i_{\mathrm{d}}}{\mathrm{d}t} = u'_{\mathrm{d}} \\ i_{\mathrm{q}} R + L \dfrac{\mathrm{d}i_{\mathrm{q}}}{\mathrm{d}t} = u'_{\mathrm{q}} \end{cases}. \tag{5}$$

When u'_{d} and u'_{q} are used as equivalent current control variables, the d-axis and q-axis are independently controlled, and the equivalent control variables are determined by the output of the PI controller. Thus, the decoupling control of the d-axis and q-axis current can be realized.

$$\begin{cases} u'_{\mathrm{d}} = \left(k_{\mathrm{ip}} + k_{\mathrm{ii}} \dfrac{1}{S}\right)\left(i^*_{\mathrm{d}} - i_{\mathrm{d}}\right) \\ u'_{\mathrm{q}} = \left(k_{\mathrm{ip}} + k_{\mathrm{ii}} \dfrac{1}{S}\right)\left(i^*_{\mathrm{q}} - i_{\mathrm{q}}\right) \end{cases}, \tag{6}$$

where k_{ip} and k_{ii} are the proportional and integral coefficients of the current inner loop PI regulator, respectively, and i^*_{d} and i^*_{q} are the reference values of d-axis and q-axis current generated by the voltage outer loop, respectively.

The reference value of the d-axis and q-axis current generated by the voltage outer loop is:

$$\begin{cases} i^*_{\mathrm{d}} = \left(k_{\mathrm{vp}} + \dfrac{k_{\mathrm{vi}}}{S}\right)\left(U^*_{\mathrm{cd}} - U_{\mathrm{cd}}\right) \\ i^*_{\mathrm{q}} = 1 \end{cases}, \tag{7}$$

where k_{vp} and k_{vi} are the proportional and integral coefficients of the voltage outer loop PI regulator, respectively.

Because the equivalent resistance R is relatively small, it is neglected here. From Eqs. (5) and (6), the change rate of i_{d} and i_{q} can be obtained as:

$$\begin{cases} \dfrac{\mathrm{d}i_{\mathrm{d}}}{\mathrm{d}t} = \left(k_{\mathrm{ip}} + \dfrac{k_{\mathrm{ii}}}{S}\right)\left(i^*_{\mathrm{d}} - i_{\mathrm{d}}\right) \\ \dfrac{\mathrm{d}i_{\mathrm{q}}}{\mathrm{d}t} = \dfrac{\left(k_{\mathrm{ip}} + \dfrac{k_{\mathrm{ii}}}{S}\right)\left(i^*_{\mathrm{q}} - i_{\mathrm{q}}\right)}{L} \end{cases}. \tag{8}$$

Because the d-axis and q-axis are symmetrical, the control of the d-axis current only is discussed below. Ignoring all disturbances, the control block diagram of the d-axis current is shown in Fig. 2.

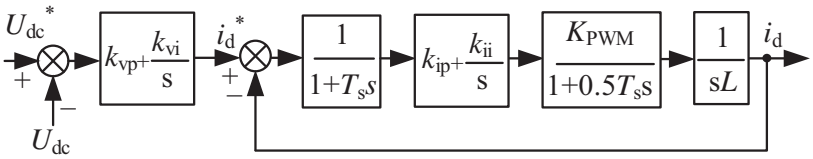

Fig. 2. Control block diagram of the d-axis current

In Fig. 2, the rectifier is replaced by a first-order inertial link. T_s is the unit sampling time, and K_{PWM} is the equivalent gain of the rectifier. Because the actual control system is discrete, Eq. (7) after discretization is:

$$i_d^*(n) = k_{vp}\, e_v(n) + k_{vi}\, T_s \sum_{j=0}^{n} e_v(j), \tag{9}$$

where $e_v(j)$ is the error signal between the given value of voltage and the j^{th} sampling value of voltage.

The discretization expression of $e_v(j)$ is:

$$e_v(j) = U_{dc}^* - U_{dc}^*(j). \tag{10}$$

Eq. (6) after discretization is:

$$u_d'(n) = k_{ip}\, e_i(n) + k_{ii}\, T_s \sum_{j=0}^{n} e_i(j), \tag{11}$$

where $e_i(j)$ is the error signal between the reference value of the current generated by the voltage outer loop and the j^{th} sampling value of the current.

$e_i(j)$ is:

$$e_i(j) = i_d^*(j) - i_d(j). \tag{12}$$

From Eqs. (8) and (11), the current change rate at the n^{th} sampling time after discretization can be obtained as:

$$\frac{\Delta i_d(n)}{T_s} = \frac{k_{ip}\, e_i(n) + k_{ii}\, T_s \sum_{j=0}^{n} e_i(j)}{L}, \tag{13}$$

where $\Delta i_d(n)$ is the error of the n^{th} and $(n-1)^{th}$ current sampling values, $\Delta i_d(n) = i_d(n) - i_d(n-1)$.

When the three-phase VSR is started, the error between the given reference voltage U_{dc}^* and the actual value U_{dc} is large, because the capacitor voltage is zero. Under the action of an outer-loop PI regulator, Eq. (10) shows that the given value of the current is far greater than the rated current, or even reaches the limit value. Because the value of i_q is zero at starting time, the current error is very large. Generally, the inner current loop is required to have a higher response speed, so the proportional and integral coefficients of the inner PI controller are usually large. In these cases, it is known from Eq. (11) that the value of the equivalent control variable is large under the action of PI regulation in the inner loop.

When pulse width modulation (PWM) or space vector PWM (SVPWM) is used, the modulation ratio is higher than the rated value, and there can even be overmodulation, which makes the initial duty cycle larger. Because a large-capacity capacitor is usually connected in parallel on the DC side of the VSR, it is charged rapidly at the start-up time, so the current change rate is very large. The existence of inductance L can restrain the inrush current to some extent; however, the value of inductance L of the VSR with high switching frequency is very small, so it cannot effectively suppress the peak value of the starting inrush current to a reasonable range. Therefore, in a short time, the value of the inrush current is still large, even far exceeding the rated current.

Ignoring the disturbance, sampling delay, and small inertia of PWM, the closed-loop transfer function of the current inner loop can be obtained from Fig. 2 as:

$$G(s) = \frac{k_{\mathrm{ip}} K_{\mathrm{PWN}} \left(s + \dfrac{k_{\mathrm{ii}}}{k_{\mathrm{ip}}} \right)}{Ls^2 + k_{\mathrm{ip}} K_{\mathrm{PWN}} s + \dfrac{k_{\mathrm{ii}}}{K_{\mathrm{PWN}}}} . \tag{14}$$

It is known from Eq. (14) that the current inner-loop controller is a second-order system with a zero point, and its damping ratio and the frequency of undamped oscillation angle are:

$$\xi_{\mathrm{n}} = \frac{k_{\mathrm{ip}} K_{\mathrm{PWN}}}{2\omega_{\mathrm{n}} L}, \qquad \omega_{\mathrm{n}} = \sqrt{\frac{k_{\mathrm{ii}} K_{\mathrm{PWN}}}{L}} . \tag{15}$$

The magnitude of overshoot mainly depends on the damping ratio. The three-phase VSR is usually operated in the underdamped state ($\xi_{\mathrm{n}} = 0.4 \sim 0.8$), and generally the value is 0.707.

When the current feedback signal rises to the given reference signal generated by the voltage outer loop, it overshoots because of the accumulation of the previous error, and this leads to a greater inrush current. With large-scale power electronic converters being connected to the grid, more and more stringent requirements are put forward for the quality of grid-connected current. However, the inrush current problem in the start-up process of power electronic converters cannot be ignored. Therefore, it is necessary to propose new control strategies that can effectively suppress the inrush current and increase the stability of the start-up process.

3. Novel strategy for suppressing the inrush current based on virtual resistor control

To suppress effectively the inrush current of a three-phase VSR during the start-up process, it is necessary to improve the control scheme. The simplest and most effective way to suppress the impulse current is to connect the start-up resistor (SR) to increase the damping of the system at start-up time, as shown in Fig. 1. After the start-up process, the start resistor is removed by a contactor. Take VT1 and VT6 as examples to analyze the suppression process of the inrush current after adding a start-up resistor.

The equivalent circuit when VT1 and VT6 are on, ignoring the equivalent resistance of the AC side, is shown in Fig. 3.

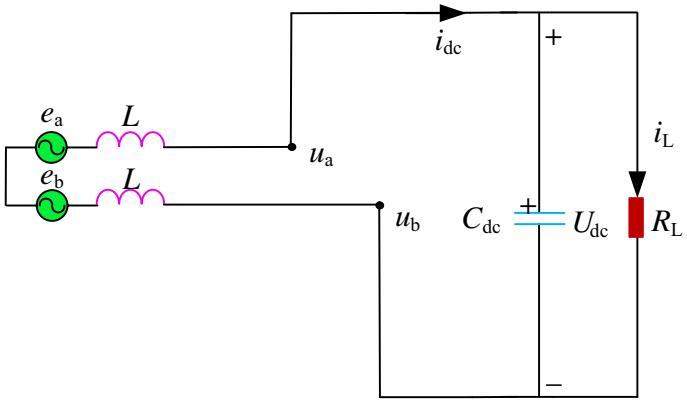

Fig. 3. Equivalent circuit when VT1 and VT6 are on

When the VSR is started, the capacitor is charged rapidly, and the capacitor voltage rises rapidly. In general, the load impedance is much larger than the capacitance reactance, so the load impedance is ignored here. Thus, the expression of i_{dc} can be obtained as:

$$i_{\mathrm{dc}} \frac{e_{\mathrm{a}} - e_{\mathrm{c}}}{2jX_{\mathrm{L}} - \dfrac{jX_{\mathrm{C}}R_{\mathrm{L}}}{(R_{\mathrm{L}} + jX_{\mathrm{C}})}} \approx \frac{e_{\mathrm{a}} - e_{\mathrm{c}}}{2jX_{\mathrm{L}} - jX_{\mathrm{C}}}, \tag{16}$$

where X_{L} and X_{C} are the values of inductance reactance and capacitance reactance, respectively.

When the startup resistor is added, the equivalent circuit is as shown in Fig. 4. At this point, Eq. (16) is changed into

$$i_{\mathrm{dc}} \frac{e_{\mathrm{a}} - e_{\mathrm{c}}}{2jX_{\mathrm{L}} - \dfrac{jX_{\mathrm{C}}R_{\mathrm{L}}}{(R_{\mathrm{L}} + jX_{\mathrm{C}})} + 2R_{\mathrm{d}}} \approx \frac{e_{\mathrm{a}} - e_{\mathrm{c}}}{2jX_{\mathrm{L}} - jX_{\mathrm{C}} + 2R_{\mathrm{d}}}. \tag{17}$$

It can be found from Eq. (17) that the charging speed of the capacitor decreases significantly after adding the startup resistor, and this can effectively reduce the magnitude of the inrush current.

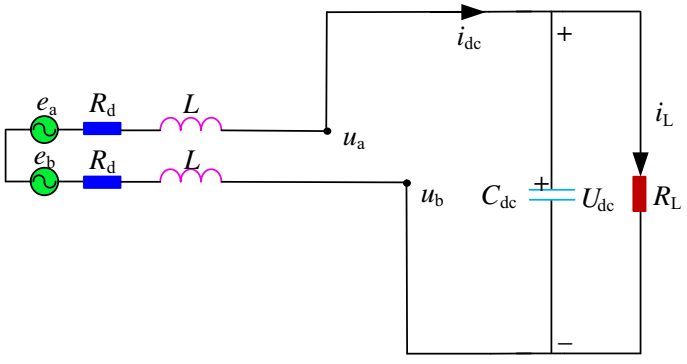

Fig. 4. Equivalent circuit when startup resistor is added

However, the introduction of the resistance and auxiliary switch increases the cost, volume, and weight of the system. In addition, because the SR consumes part of the voltage in the operation process, it increases the system loss and makes the capacitive current rise again when it is cut off. This affects the system again, so it needs to be improved.

To avoid increasing the system loss, the active damping control strategy, which replaces the actual resistor, has attracted wide attention in academic circles. Pekik Argo Dahono first proposed a "virtual resistor" control algorithm to replace the actual resistor. Its basic idea is to transform the control structure diagram containing the resistor into an equivalent one and to replace the actual resistor with a control algorithm.

The d-axis control block diagram after adding the startup resistor is shown in Fig. 5. Fig. 6 can be obtained by separating the startup resistor term. According to the equivalent transformation rule of the control structure in the principle of automatic control, the control block diagram of the d-axis current with a virtual resistor can be obtained from Fig. 6. It is shown in Fig. 7.

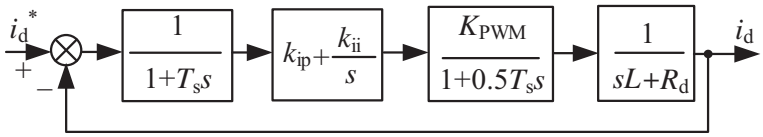

Fig. 5. Control block diagram of d-axis current with startup resistor

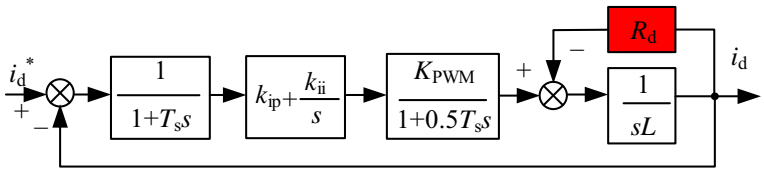

Fig. 6. Control block diagram of d-axis current with separated startup resistor

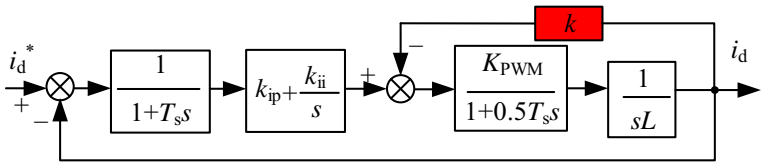

Fig. 7. Control block diagram of d-axis current with virtual resistor

According to the equivalent transformation rule, the value of k can be calculated as follows after neglecting the small inertia link of the VSR:

$$k = \frac{R_d}{K_{PWM}}. \tag{18}$$

Because the above transformation is equivalent, it does not change the transient performance of the system. From Fig. 7, the realization method of the virtual resistor can be clearly analyzed.

It is to add a current component with a value of ki_d to the output value of the PI controller. This method can directly be achieved by an algorithm, so it is simple to implement.

When a virtual resistor is added, Eq. (11) is changed into:

$$u'_\mathrm{d} = \left(k_\mathrm{ip} + k_\mathrm{ii}\frac{1}{S}\right)\left(i^*_\mathrm{d} - i_\mathrm{d}\right) - ki_\mathrm{d}\,. \tag{19}$$

Eq. (19) is discretized into:

$$u'_\mathrm{d}(n) = k_\mathrm{ip}\,e_\mathrm{i}(n) + k_\mathrm{ii}\,T_\mathrm{s}\sum_{j=0}^{n} e_\mathrm{i}(j) - ki_\mathrm{d}(n). \tag{20}$$

When virtual resistance is added, Eq. (8) is changed into:

$$\frac{\mathrm{d}i_\mathrm{d}}{\mathrm{d}t} = \frac{\left(k_\mathrm{ip} + \dfrac{k_\mathrm{ii}}{S}\right)\left(i^*_\mathrm{d} - i_\mathrm{d}\right) - ki_\mathrm{d}}{L}\,. \tag{21}$$

Eq. (21) is discretized into:

$$\frac{\Delta i_\mathrm{d}(n)}{T_\mathrm{s}} = \frac{k_\mathrm{ip}\,e_\mathrm{i}(n) + k_\mathrm{ii}\,T_\mathrm{s}\displaystyle\sum_{j=0}^{n} e_\mathrm{i}(j)}{L} - \frac{ki_\mathrm{d}(n)}{L}\,. \tag{22}$$

When the virtual resistor is added, it can be seen from Eq. (20) that the equivalent control variable u'_d decreases, and Eq. (22) shows that the current change rate decreases. This shows that adding virtual resistance can restrain the rising speed of the inrush current, so it can effectively reduce the inrush current.

Unlike the starting resistance, which directly suppresses the inrush current by consuming part of the electric energy, the virtual resistance method controls the charging time on the DC side by reducing the equivalent control variables, thus changing the duty cycle of the starting time and delaying the charging process to reduce the current on the grid side. Ignoring the disturbance, sampling delay, and small inertia of PWM, the closed-loop transfer function of the current inner loop can be obtained from Fig. 7 as:

$$G_\mathrm{ci}(s) = \frac{k_\mathrm{ip}\,K_\mathrm{PWM}\left(s + \dfrac{k_\mathrm{ii}}{k_\mathrm{ip}}\right)}{Ls^2 + \left(kK_\mathrm{PWM} + k_\mathrm{ip}\,K_\mathrm{PWM}\right)s + k_\mathrm{ii}\,K_\mathrm{PWM}}\,. \tag{23}$$

The system damping ratio is changed into:

$$\xi_\mathrm{n} = \frac{\left(k + k_\mathrm{ip}\right)K_\mathrm{PWM}}{2\omega_\mathrm{n}L}\,. \tag{24}$$

Eq. (24) shows that when the virtual resistance is introduced, the damping ratio of the system increases, and this can reduce the current overshoot, thus effectively suppressing the inrush current.

From the above analysis, it is known that the inrush current can be suppressed by adding the start-up resistor, but this inevitably causes a certain impact on the system during the removal process. The virtual resistor can simulate the actual resistor, but, unlike the actual resistor, the virtual resistor can be realized by an algorithm, and its value can be changed in real time. Therefore, if the virtual resistor control method can be reasonably designed, not only can the inrush current be effectively suppressed, but the impact on the system is also prevented from occurring again.

For this purpose, the value of k can be reduced to zero at a fixed slope instead of being set to a fixed value. The curve of k is shown in Fig. 8. A block diagram of the SVPWM three-phase VSR with a virtual resistor is shown in Fig. 9.

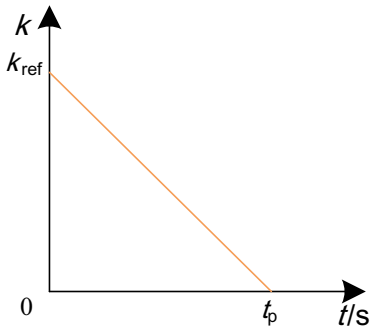

Fig. 8. Curve of k

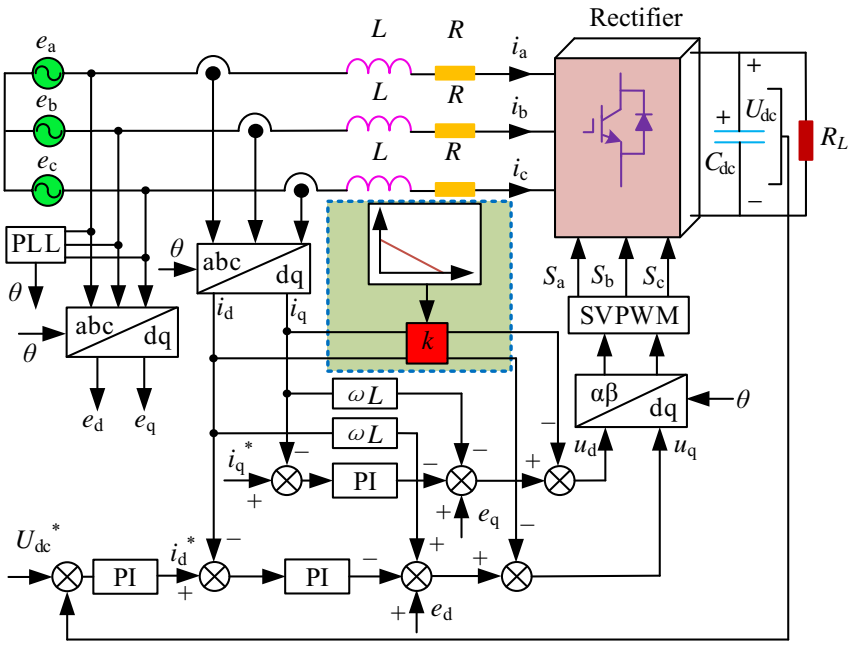

Fig. 9. Block diagram of the SVPWM three-phase VSR with virtual resistor

The curve equation of k is:

$$k = k_{\text{ref}} - \frac{k_{\text{ref}}}{t_{\text{p}}} t, \tag{25}$$

where k_{ref} is the initial given value, and t_{p} is the time it takes for the capacitor voltage to rise to the rated value.

4. Simulation and experimental verification

To verify the accuracy and effectiveness of the proposed method, a three-phase VSR model was established using MATLAB/Simulink. The simulation parameters are shown in Table 1.

Table 1. Main parameters

Parameter name	Symbol	Value	Unit
Amplitude of AC voltage	e_{abc}	130	V
Frequency of AC voltage	f	50	Hz
DC voltage	U_{dc}	350	V
DC capacitance	C_{dc}	1000	μF
AC side resistance	R	0.1	Ω
AC side inductance	L	5	mH
Load resistance	R_{L}	30	Ω
Switching frequency	f_{s}	10	kHz
Outer loop proportional coefficient	k_{vp}	0.05	
Outer loop integral coefficient	k_{vi}	15	
Inner loop proportional coefficient	k_{ip}	30	
Inner loop integral coefficient	k_{ii}	500	
PWM equivalent gain	k_{PWM}	1	

Fig. 10(a) shows that the value of the equivalent control variable u'_{d} at start-up time is very large, and this can cause overmodulation. The pulse signals of switches VT1, VT3, and VT5 are shown in Figs. 10(b), (c), and (d), respectively. There is indeed a short period of overmodulation observed, which causes the capacitor to be charged quickly by two phases in a three-phase power supply. Its equivalent circuit can refer to Fig. 4 at this time.

The waveforms of capacitive current, capacitive voltage, and three-phase AC side current are shown in Figs. 10(e), (f), and (g), respectively. Figs. 10(e) and (f) show that the capacitive current rises rapidly at the start-up time, with a maximum of 64 A. With the rapid charging of the capacitors, the capacitor voltage also rises rapidly, and it soon reaches the rated value. Because of the regulating effect of the PI regulator, there is a small overshoot. Fig. 10(g) shows

that the amplitude of the three-phase AC current during start-up time can reach 66 A, which is approximately three times as much as the rated current. At this time, if the current margin of the power electronic devices is small, it leads to device damage and triggers overcurrent protection, which affects the system. After the capacitor voltage rises to the rated value, the capacitor enters a stable charging and discharging state, and the system also enters a stable operation state.

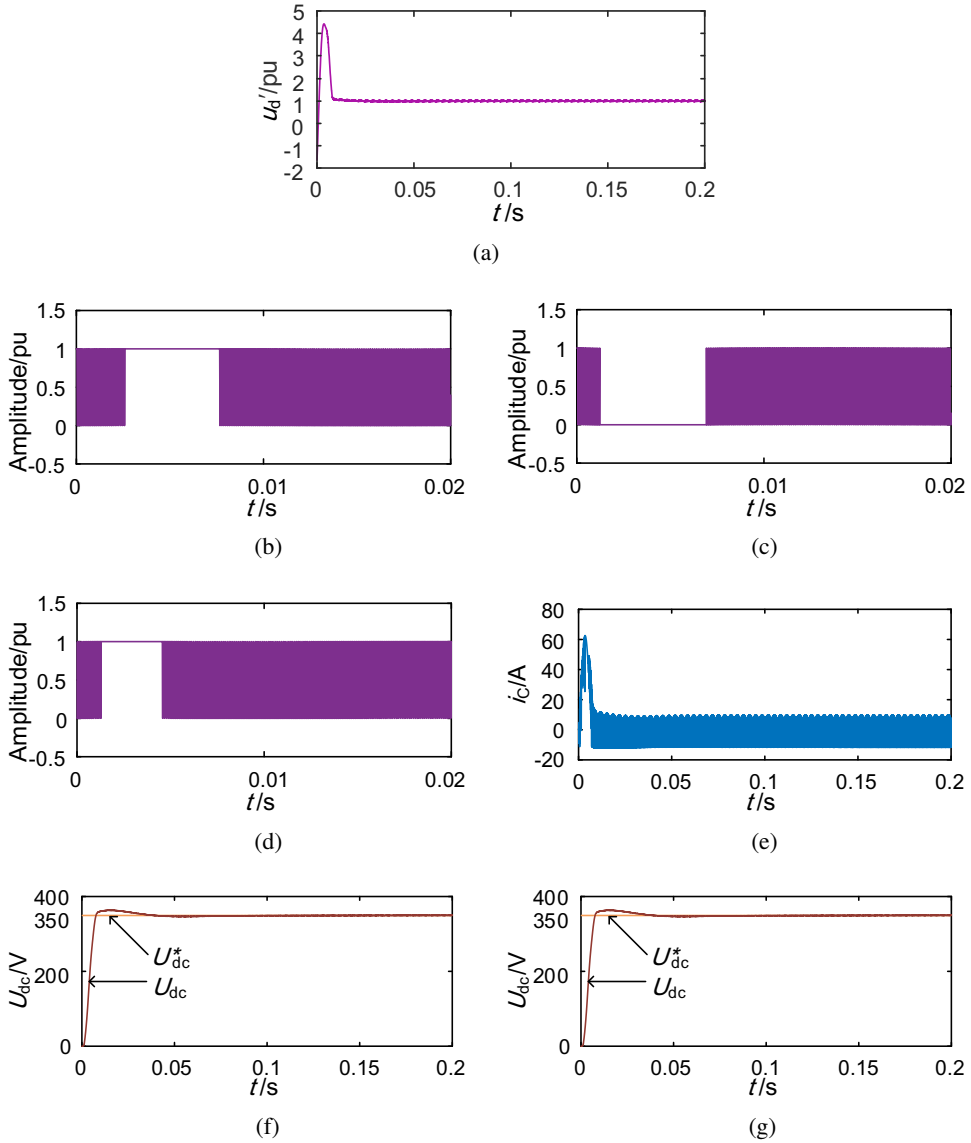

Fig. 10. No measures to suppress inrush current: (a) waveform of u'_d; (b) pulse signal of switch S_1; (c) pulse signal of switch S_3; (d) pulse signal of switch S_5; (e) waveform of capacitive current; (f) waveform of capacitive voltage; and (g) waveform of AC side current

To verify the suppression effect of the start-up resistor, a 5-Ω start-up resistor was added at the start-up time and removed in 0.01 s as an example.

The waveforms of capacitive current, capacitive voltage, and three-phase AC side current are shown in Figs. 11(a), (b), and (c), respectively. The peak value of capacitive current was reduced to 24 A. At 0.01 s, the capacitive voltage rose to 300 V. After the start-up resistor was removed, the capacitive current increased rapidly to 34 A, and the capacitor voltage rose to 350 V. Fig. 11(c) also shows that the inrush current was generated again after the starting resistance was removed. These results show that the start-up resistor can restrain the inrush current, but, because the SR consumes part of the voltage, it has a certain impact on the system again when it is removed.

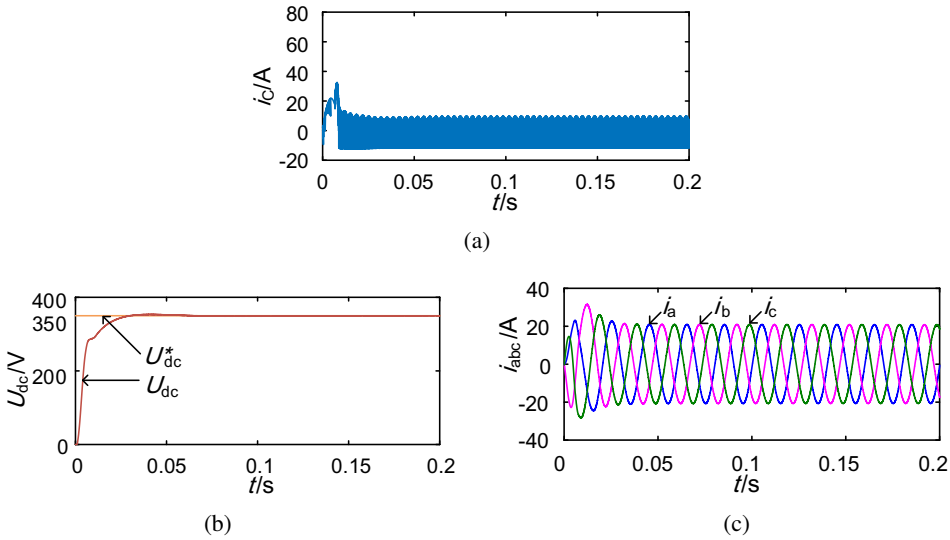

Fig. 11. Adding start-up resistor: (a) waveform of capacitive current, (b) waveform of capacitive voltage, and (c) waveform of AC side current

To verify the effectiveness of the virtual resistor control strategy, k_{ref} is 5 and t_p is 0.02 s as an example.

The waveform of u'_d is shown in Fig. 12(a) for when the virtual resistor was added. The equivalent control variables were effectively reduced, and the overmodulation phenomenon was suppressed. The waveforms of capacitive current, capacitive voltage, and three-phase AC side current are shown in Figs. 12(b), (c), and (d), respectively. As Fig. 12(e) shows, the maximum capacitive current was 22 A, and then it slowly entered a stable charging and discharging state. Fig. 12(f) shows that the rising process of capacitive voltage was more stable, and Fig. 12(g) shows that the inrush current of the three-phase AC side was effectively suppressed, and the current quality was effectively improved.

To verify the effectiveness of the proposed control strategy further, experiments were carried out on the experimental platform, and the experimental parameters were consistent with the simulation parameters. A photograph of the experimental platform is shown in Fig. 13. The TMS320F28335 DSP was chosen as the embedded platform.

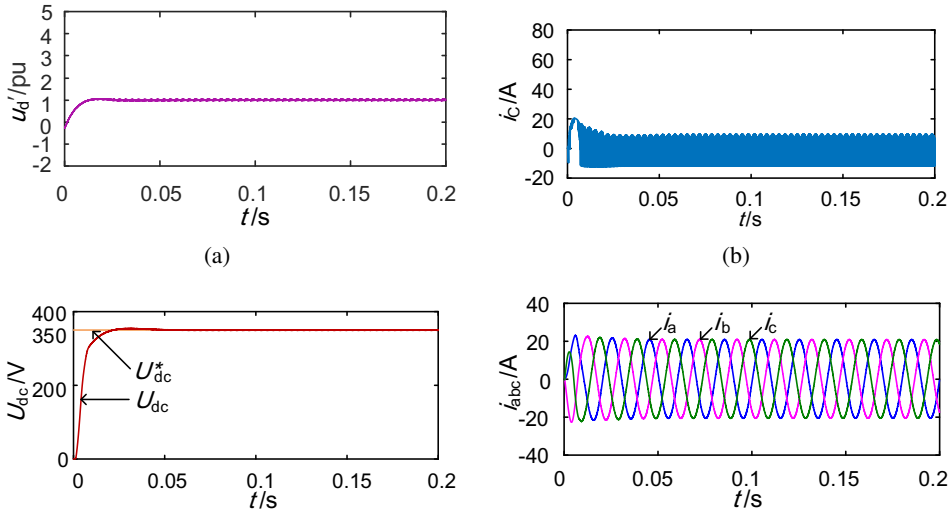

Fig. 12. No measures to suppress inrush current: (a) waveform of u'_d; (b) waveform of capacitive current; (c) waveform of capacitive voltage; and (d) waveform of AC side current

Fig. 13. Photograph of the experimental platform

Fig. 14 shows the experimental waveforms without any measures to suppress the inrush current. It can be seen that a large inrush current could be generated at the start-up moment with a value of 56 A. This value is slightly lower than the simulation value, because the parasitic resistance was not considered in the simulation. If the current margin of power electronic devices is small, the device can be damaged, and the overcurrent protection is triggered, which affects the system. Fig. 15 shows the current waveforms after a start-up resistor was added. It can be seen

that the inrush current is suppressed at the start-up moment, but a smaller inrush current appeared again when the start-up resistor was removed. Fig. 16 shows the current waveforms after a virtual resistor was added. There was almost no start-up inrush current. These experimental results are basically consistent with the simulation results. Therefore, the accuracy and effectiveness of the proposed control strategy were verified.

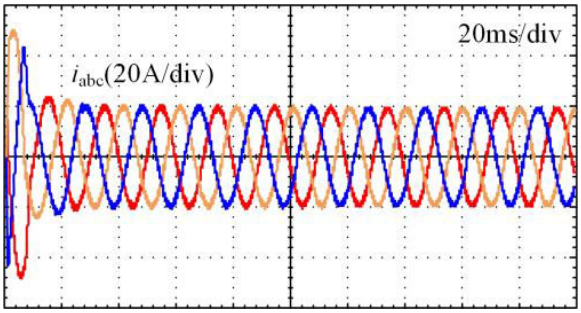

Fig. 14. Experimental waveforms of three-phase grid-connected current when there is no way to add

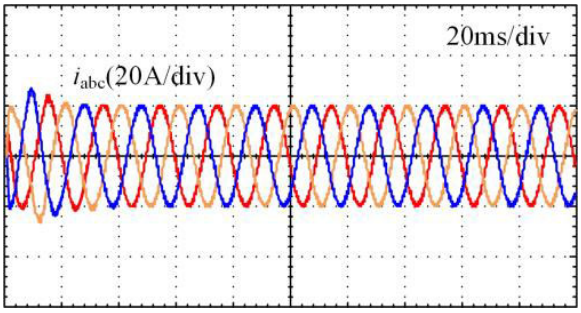

Fig. 15. Experimental waveforms of three-phase grid-connected current after adding the start-up resistor

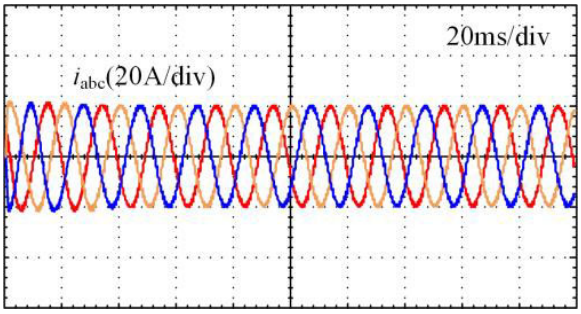

Fig. 16. Experimental waveforms of three-phase grid-connected current after adding the virtual resistor

To highlight the advantages of the methods proposed, a detailed comparison of the main existing methods was made, as shown in Table 2. The method proposed in this paper has obvious advantages over the existing methods: it does not need to increase hardware costs, there is no secondary inrush current, and the sensitivity of the parameters and the complexity of control are low.

Table 2. Comparison of various methods

Method	Cost	Secondary inrush current	Sensitivity of parameters	Complexity of control
Start-up resistor [12]	Resistors and switches	Yes	Low	Low
Slow ramp reference value [5–7]	No	No	High	Low
[8–11, 13, 14]	Voltage and current sensors	No	Low	High
Virtual resistor	No	No	Low	Low

5. Conclusions

1. The reason for the inrush current of the three-phase VSR is that the error between the given reference voltage and the actual value is large during start-up time. Under the action of PI regulation, the equivalent control variable is too large, and the capacitor charges quickly.
2. In this study, a new strategy for suppressing the inrush current based on virtual resistor control was proposed. It can be realized directly by adding an algorithm to the controller. Compared with the starting resistor method, this method is simple to implement. It does not cause an impact on the system again, and it can improve the dynamic quality of the grid side current.
3. The formation of the starting inrush current of grid-connected inverters is similar to that of a VSR, so the strategy proposed can be extended to suppress the inrush current of grid-connected inverters.
4. The simulation and experimental results show that the proposed method can restrain inrush current effectively and has obvious advantages over the existing methods.

References

[1] Kouro S., Leon J.I., Vinnikov D., *Grid-connected photovoltaic systems: an overview of recent research and emerging PV converter technology*, IEEE Industrial Electronics Magazine, vol. 9, no. 1, pp. 47–61 (2015).

[2] Zeng Zheng, Zhao Rongxiang, Tang Shengqing, *An overview on advanced grid-connected inverters used for decentralized renewable energy resources*, Proceedings of the CSEE, vol. 33, no. 24, pp. 1–12 (2013).

[3] Pena R., Cardenas R., Asher G., *Overview of control system s for the operation of DFIGs in wind energy applications*, IEEE Transactions on Industrial Electronics, vol. 60, no. 7, pp. 2776–2798 (2013).

[4] Bialasiewicz J.T., *Renewable energy systems with photovoltaic power generators: operation and modelling*, IEEE Transactions on Industrial Electronics, vol. 55, no. 7, pp. 2752–2758 (2008).

[5] Deng Wenlang, Hu Bihua, Guo Yougui, *Grading startup control for three-phase voltage-source PWM rectifier*, Power Electronics, vol. 48, no. 1, pp. 30–32 (2014).

[6] Liu Bo, Ben Hongqi, Bai Yinlong, *A slow given method to suppress the start-up inrush current of PWM rectifier*, Transactions of China Electrotechnical Society, vol. 33, no. 12, pp. 2758–2766 (2018).

[7] Yao Zhilei, Xiao Lan, *Soft-start control for SVPWM-based three-phase grid-connected inverters*, High Voltage Engineering, vol. 39, no. 11, pp. 2750–2755 (2013).

[8] Kumar M., Huber L., Jovanovic M.M., *Startup procedure for DSP-controlled three-phase six-switch Boost PFC rectifier*, IEEE Transactions on Power Electronics, vol. 30, no. 8, pp. 4514−4523 (2015).

[9] Xu Sheng, *Novel current overshooting control strategy for PWM rectifier starting*, Chinese Journal of Power Sources, vol. 39, no. 1, pp. 158–160 (2015).

[10] He Jinping, Jun Yjin, *Analysis of start-up inrush current and its mitigation control strategy for grid connected voltage source inverter*, Research in Veterinary Science, vol. 96, no. 1, pp. 153−159 (2014).

[11] Qi Qi, Xiao Lan, *A method of soft starting of three-phase voltage source PWM rectifier*, Power Electronics, vol. 48, no. 2, pp. 24–27 (2014).

[12] Zhong Chen, Du Haijiang, Yang Minghao, *Analysis of starting inrush current of three-phase unity power factor VSR and its suppression*, Power Electronics, vol. 47, no. 5, pp. 32–34 (2013).

[13] Li Jie, Song Wenxiang, Ma Yiwei, *Improvement of starting performance for three-phase PWM grid-connected inverter based on phase and amplitude control*, Transactions of China Electrotechnical Society, vol. 24, no. 4, pp. 152–156 (2009).

[14] Yang Liang, Wang Zong, Lv ZhiPeng, *The method of pre-synchronized grid-connection of synchronverter*, Power System Technology, vol. 38, no. 11, pp. 3203–3108 (2014).